A Generalized Inverse Method for Testing Depth-Dependent Extension Models at Highly Extended Continental Margins*

Alistair Crosby[1], Nicky White[2], Glyn Edwards[1], Mark Thompson[1], Richard Corfield[1], and Laura Mackay[1]

Search and Discovery Article #30210 (2011)
Posted December 12, 2011

*Adapted from extended abstract prepared in conjunction with oral presentation at AAPG International Conference and Exhibition, Milan, Italy, October 23-26, 2011

[1]BP Exploration, London, United Kingdom (alistair.crosby@uk.bp.com)
[2]Bullard Laboratories, University of Cambridge, Cambridge, United Kingdom

Abstract

A general understanding of rifted margins, which form by thinning of the continental lithosphere, exists. Nevertheless, the exact form of thinning is unclear. This debate has been stimulated by acquisition of dense seismic wide-angle and deep reflection surveys from the Atlantic Ocean margins. A central issue concerns the way in which thinning changes with depth, which has important implications for heat flow and structural styles during rifting. We have tackled this issue by developing a generalized inverse model (Figure 1 and Figure 2). This model attempts to fit tectonic subsidence, crustal thinning and melt volumes by varying strain rate as a function of time and space. Crucial inputs are present-day dynamic topography (Figure 3) and an estimate of paleo-water depth and paleo-topography through time, and it is important that these estimates are as accurate as possible. Depth-dependent thinning is permitted but we do not prescribe its existence or form beyond the requirement that mass is conserved.

We have applied the algorithm to five margins (Figures 4, 5 and 9), including two of the most contentious: Newfoundland-Iberia (Figure 5, Figure 6, Figure 7, and Figure 8) and Brazil-Angola (Figure 9, Figure 10, and Figure 11). In all cases, calculated strain rate histories predict thinning factors which broadly match estimates inferred from normal faulting and are consistent with global trends (Figure 12). Most of the margins we have studied had extension that was uniform with depth. By contrast, extension of the Newfoundland-Iberian margins occurred with a pattern of strongly depth-dependent strain rate. To account for the paucity of syn-rift decompression melting of the underlying asthenosphere, lithospheric mantle close to the ocean-continent transition must have thinned more slowly than the overlying crust. This form of depth-dependency is not common. For example, the Brazil-Angola conjugate margins could have formed by uniform lithospheric thinning

provided thick layers of salt were deposited in a pre-existing 400-600 m topographic depression. Depth-dependent thinning is not required to account for the existence of thick, unfaulted sequences of pre-salt sedimentary rocks. More generally, 2D strain rate inversion provides a powerful way to test the validity of stratigraphic interpretations during the early stages of basin screening. The results can also be used to calculate heat flow during and after rifting. Our workflow therefore reduces uncertainty in both source rock maturity and in the timing and magnitude of extension in frontier exploration basins.

References

Crosby, A., N. White, G. Edwards, and D. Shillington, 2008, Evolution of the Newfoundland-Iberia conjugate rifted margins: Earth and Planetary Science Letters, v. 273, p. 214-226.

Crosby, A.G., N.J. White, G.R.H. Edwards, and D.J. Shillington, 2010, Self-consistent strain rate and heat flow modelling of lithospheric extension: application to Newfoundland-Iberia conjugate margins: Petroleum Geoscience, v. 16, p. 247-256.

Crosby, A.G., N.J. White, G.R.H. Edwards, M. Thompson, R. Corfield, and L. Mackay, 2011, Evolution of deep-water rifted margins: Testing depth-dependent extensional models: Tectonics, v. 30, TC1004, doi:10.1029/2010TC002687.

Jones, S.M., N.J. White, P. Faulkner, and P. Bellingham, 2004, Animated models of extensional basins and passive margins: Geochemistry, Geophysics, Geosystems, v. 5, QO8009, doi:10.1029/2003GC000658.

McKenzie, D., 1978, Some remarks on the development of sedimentary basins: Earth and Planetary Science Letters, v. 40, p. 25-32.

Newman, R., and N. White, 1999, The dynamics of extensional sedimentary basins: constraints from subsidence inversion: Philosophical Transactions of the Royal Society, London, A., v. 357, p. 805-830.

Reston, T.J., 2009, The extension discrepancy and syn-rift subsidence deficit at rifted margins: Petroleum Geoscience, v. 15, p. 217-237.

Walsh, J., J. Watterson, and G. Yielding, 1991, The importance of small-scale faulting in regional extension: Nature, v. 351, p. 391-393.

Winterbourne, J., A. Crosby, and N. White, 2009, Depth, age and dynamic topography of oceanic lithosphere beneath heavily-sedimented Atlantic margins: Earth and Planetary Science Letters, v. 287, p. 137-151.

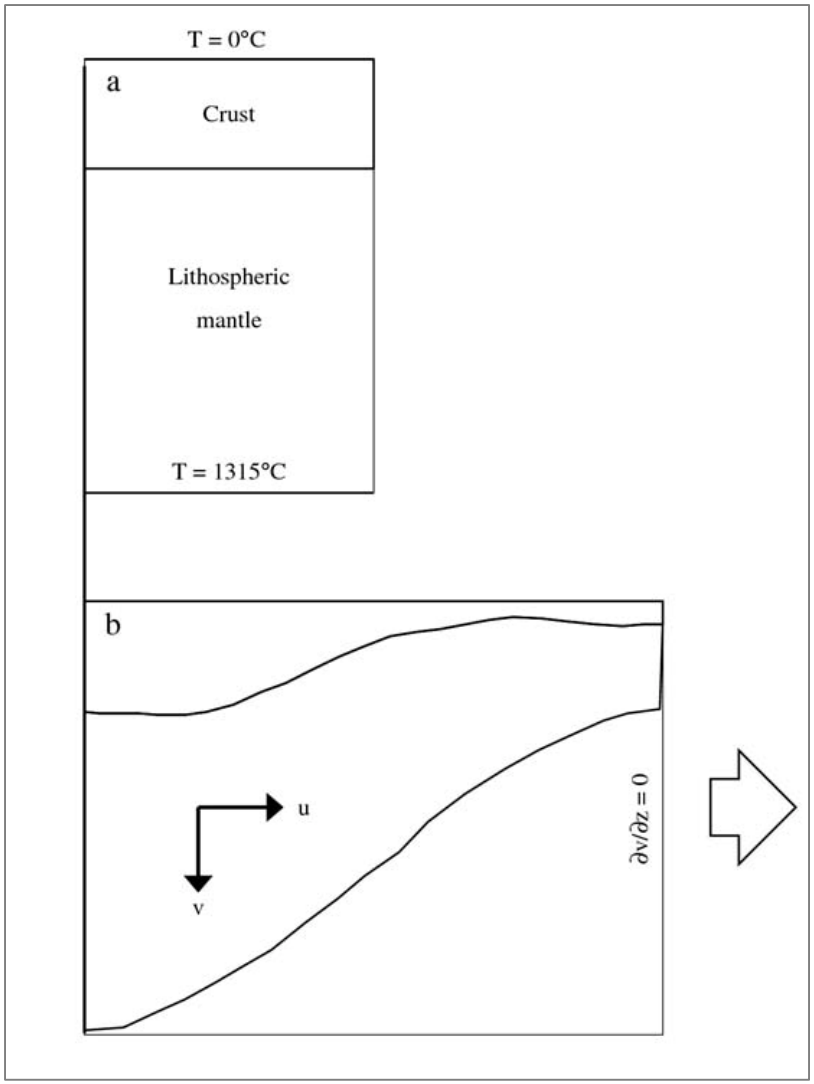

Figure 1. Illustration showing the principles that underlie the strain rate inversion algorithm. Strain rate is permitted to vary as a function of time and space within the constraints imposed by mass conservation. (a) Undeformed lithospheric template. (b) Deformed lithosphere. The crustal thickness and temperature field of the deformed lithosphere are used to calculate isostatic subsidence through time in the forward model, which is iterated to ensure an optimal fit with the observed tectonic subsidence history in the inverse algorithm. Additional constraints can be imposed to fit crustal thickness and melting observations as required.

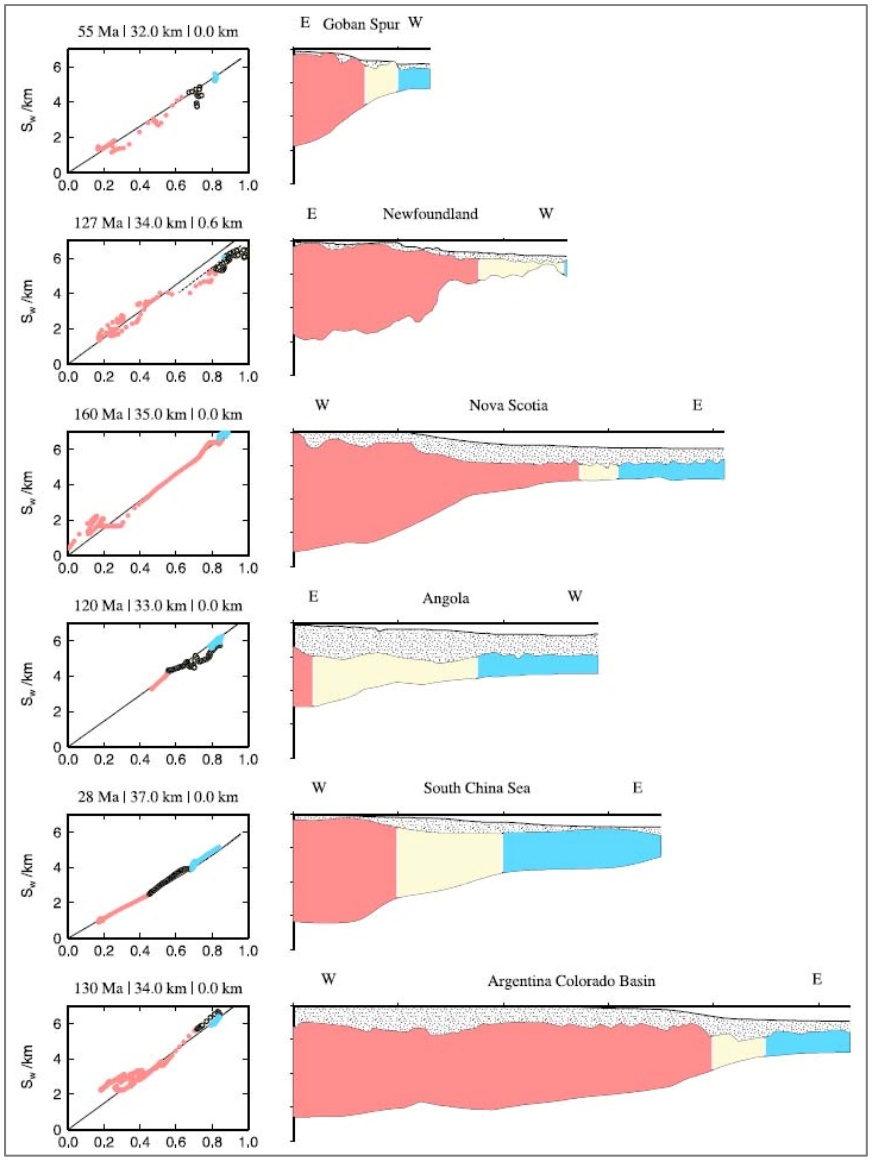

Figure 2. Test of isostasy at continental margins. Right hand panels show digitized crustal profiles from wide-angle seismic surveys. Red = bona-fide continental crust, yellow = transitional crust, blue = bona-fide oceanic crust. Left hand panels show tectonic subsidence (vertical axis) versus extension factor (horizontal axis) color-coded by crustal type. Solid line shows an isostatic model with rift age, reference crustal thickness and dynamic topographic correction indicated in the title. The agreement between theory and observation is good, which illustrates that the isostatic assumption used to calculate subsidence in this study is appropriate. For data references, see Crosby et al. (2011).

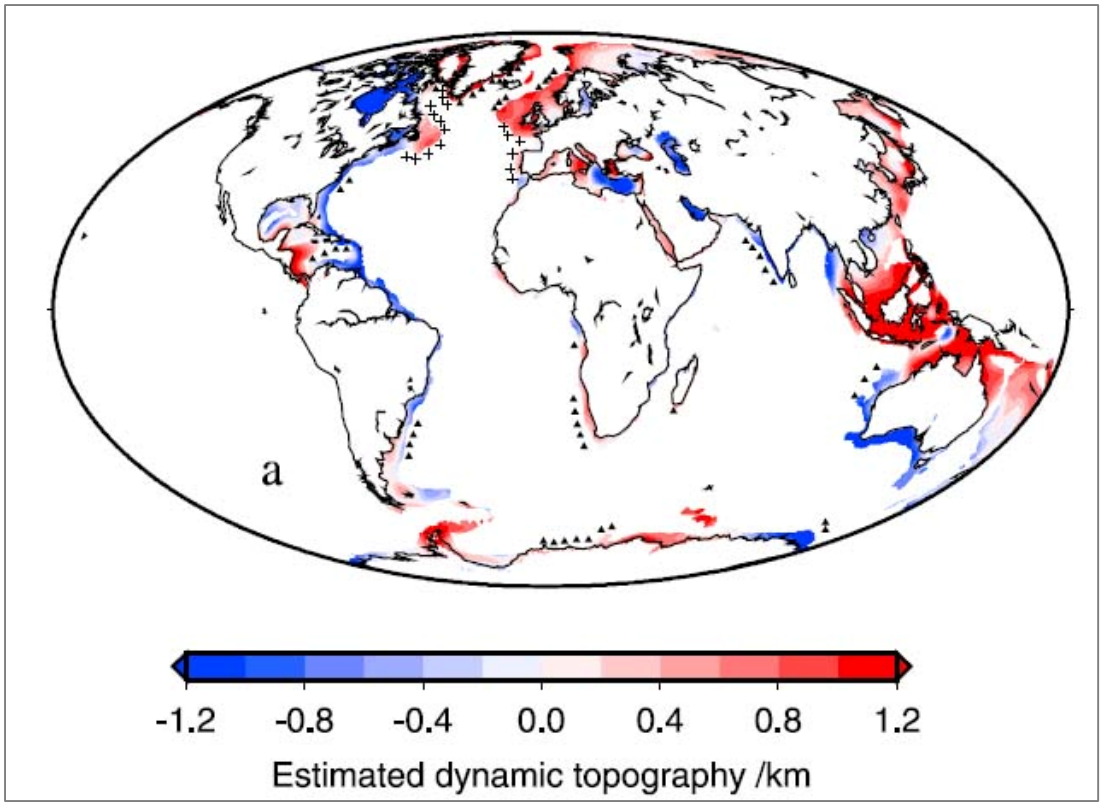

Figure 3. Dynamic topography correction estimated from global long-wavelength free-air gravity field (Winterbourne et al., 2009). Triangles = volcanic margins, crosses = cold margins with extreme crustal thinning.

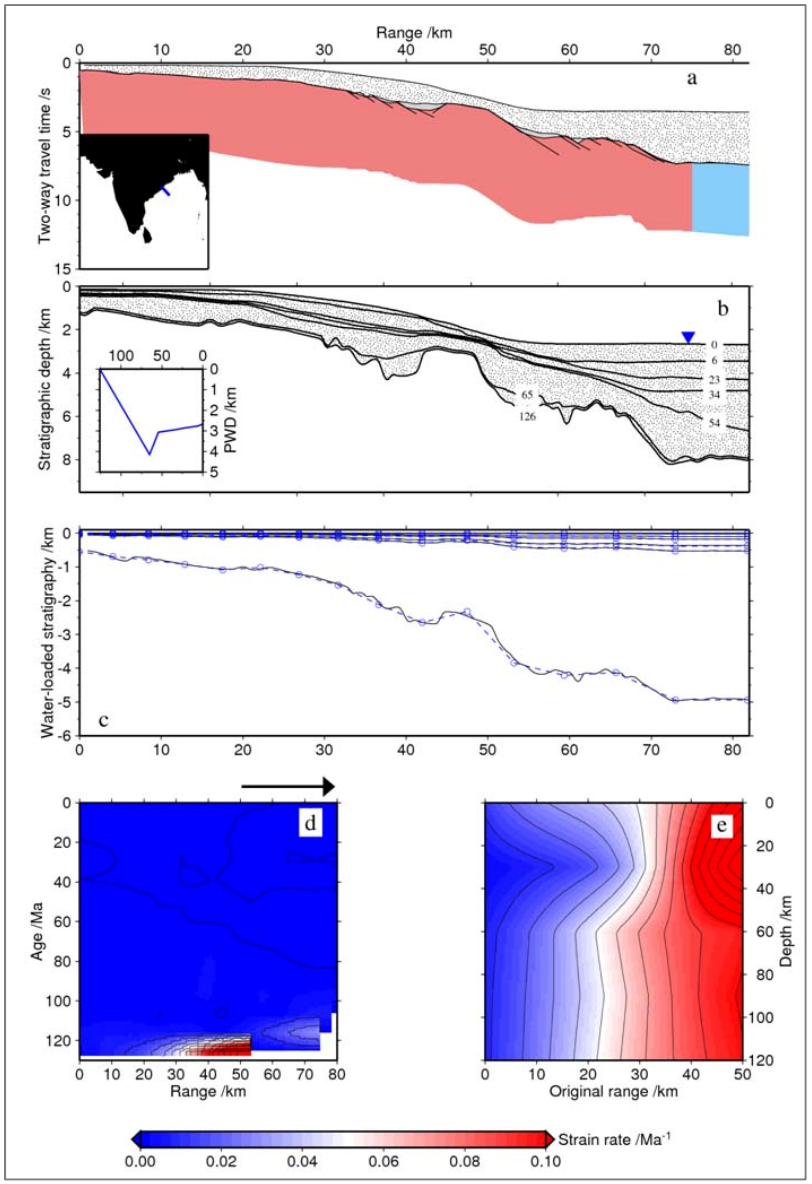

Figure 4. Example analysis of the East India margin showing simple uniform thinning of the lithosphere. (a) Interpreted structure of margin. Inset shows location. (b) Smoothed stratigraphic interpretation, with age of horizons given in Ma. Inset shows paleobathymetric template at position marked by solid triangle. (c) Tectonic subsidence. Solid lines = observed water-loaded stratigraphy, dashed lines and open circles = optimum model fit. (d) Slice through calculated cube of strain rate variation which predicts the subsidence shown in c, plotted as a function of geologic time and range along profile. Black arrow = total extension. Initial rift event followed by thermal subsidence is clearly defined. (e) Slice through calculated strain rate variation in the first time step shows that strain rate is largely invariant with depth.

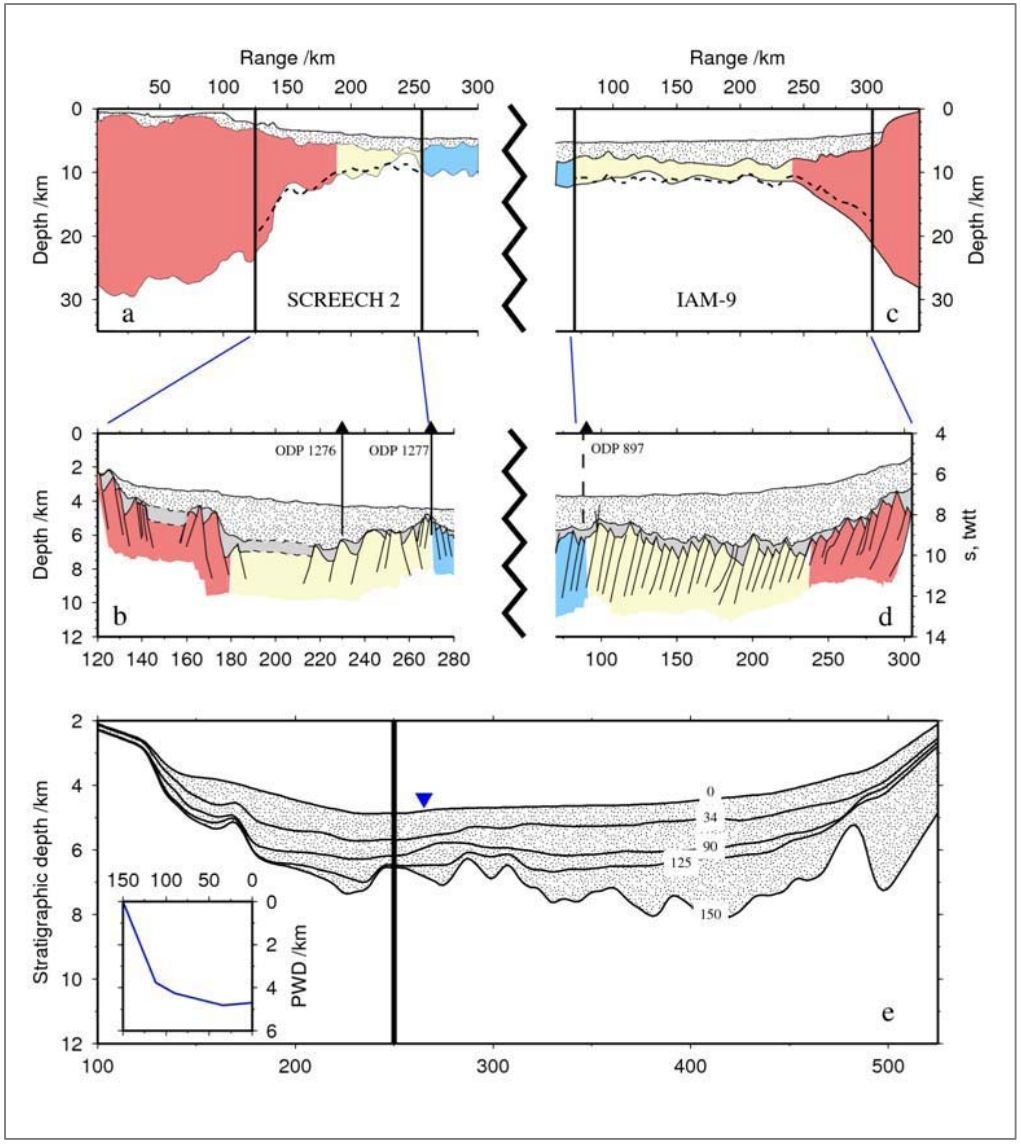

Figure 5. Conjugate Newfoundland-Iberia margins. (a) Crustal structure of SCREECH 2 line on Newfoundland side. Dashed line = best-fit model to present-day crustal structure. (b) Crustal structure of IAM-9 line on Iberian side. (c, d) Enlargements showing faulting visible in seismic reflection images and syn-rift and post-rift sediments. Vertical lines = coincident boreholes. (e) Joined stratigraphic profiles with horizon ages in Ma after correcting for differences in dynamic topography. Inset shows paleowater depth reconstruction at location marked by blue triangle. For data references, see Crosby et al. (2008, 2011).

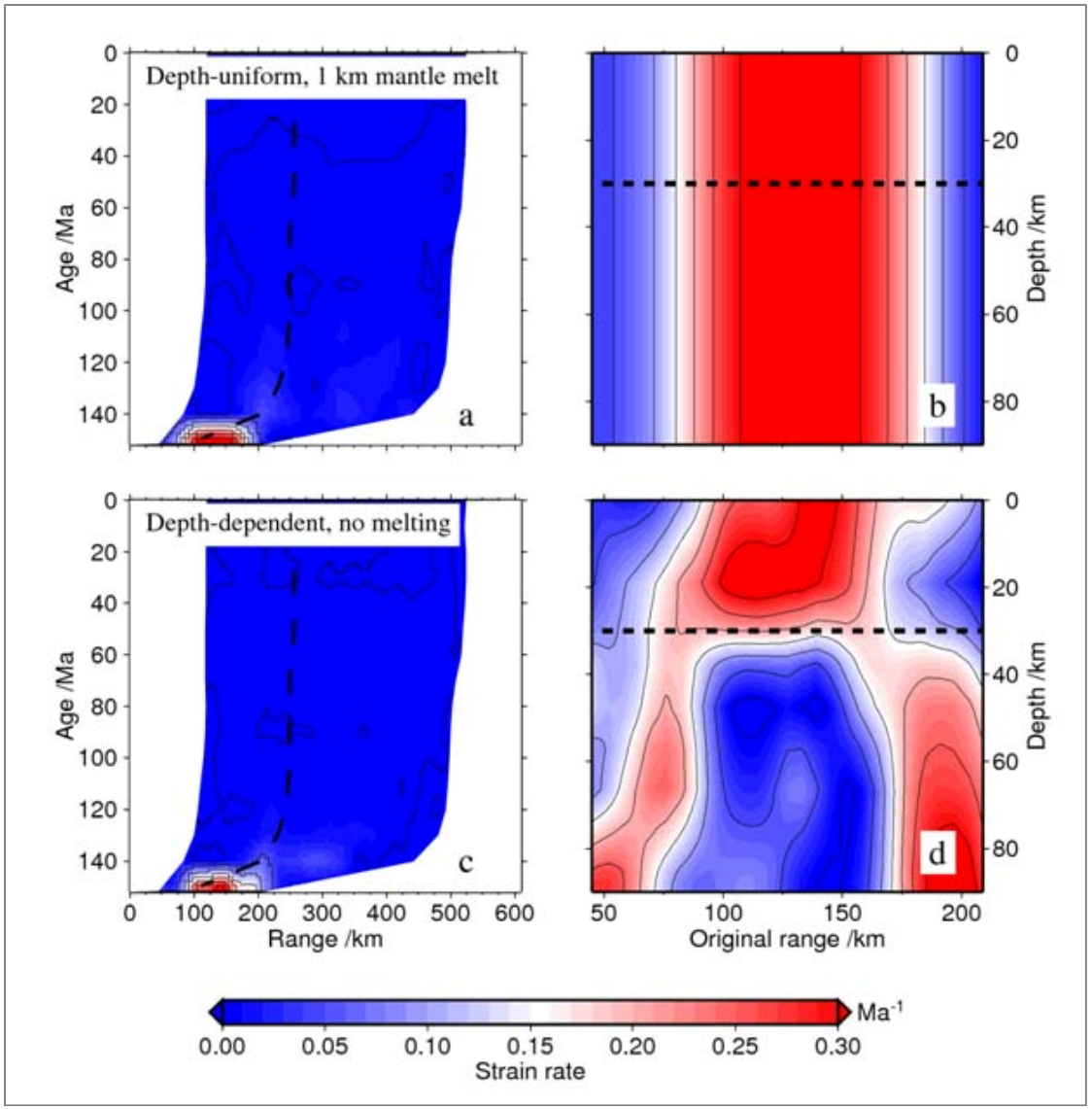

Figure 6. Strain rates corresponding to stratigraphic fits in Figure 7. (a, b) Depth-uniform strain rates. This model gives an excellent fit to the data but predicts the generation of 1 km thickness of syn-rift mantle melt which is not observed. Dashed-line = base of crust. (c, d) Depth-dependent strain rates with mantle solidus overstep penalized during the inversion. Note extreme depth dependency, which is consistent with crustal detachments near the ocean-continent transition. Total extension estimates agree with interpretations of normal faulting given the likely existence of multiple generations of faulting and the observation that up to 50% of extension may be sub-seismic (Walsh et al., 1991; Reston, 2009).

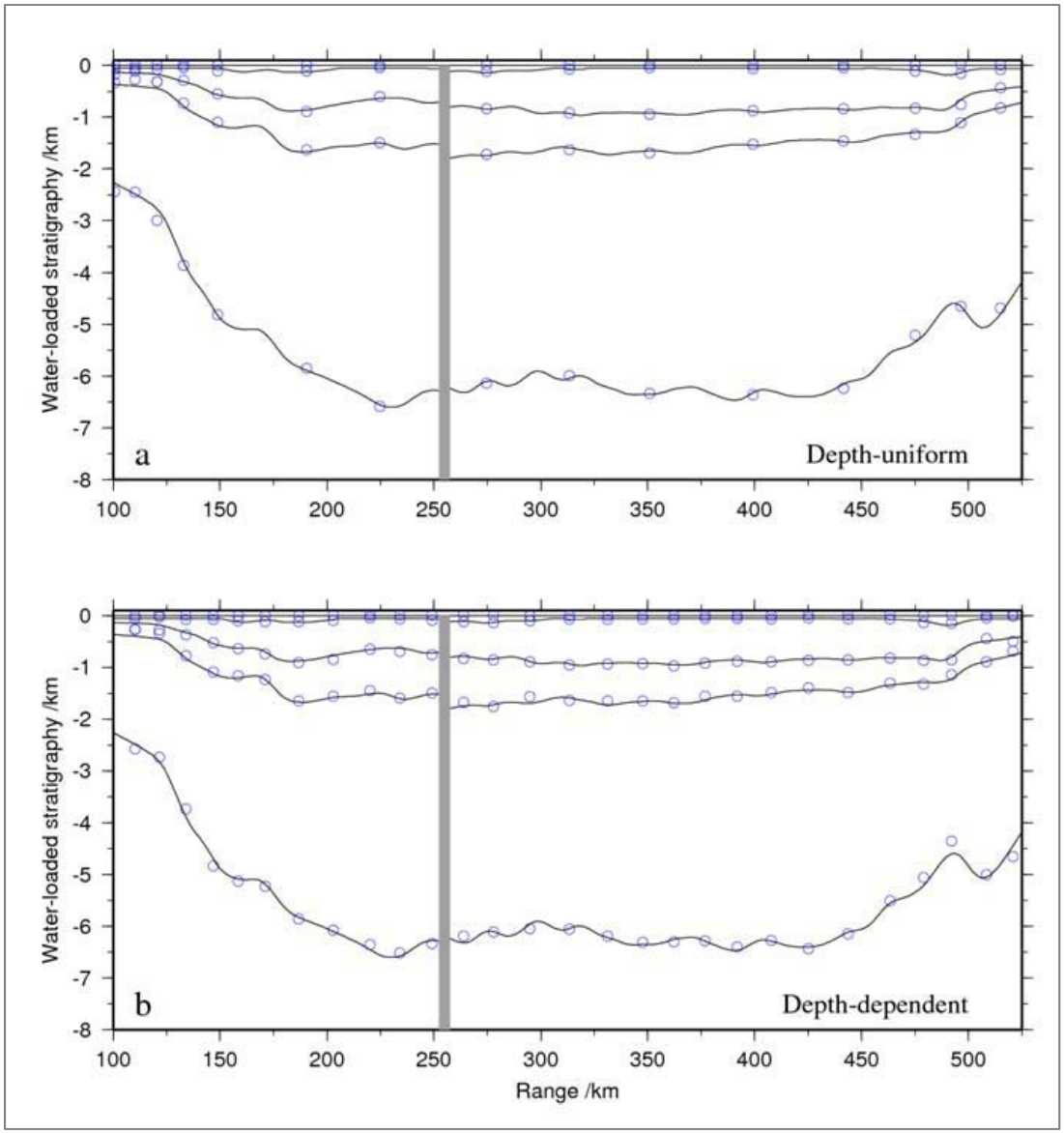

Figure 7. Reconstructed water-loaded stratigraphy for conjugate Newfoundland-Iberia lines in Figure 5. Solid line = data, circles = best-fit model. (a) Depth-uniform model in Figures 6a and 6b. (b) Depth-dependent strain rate model in Figures 6c and 6d. Fits are equally good, but depth-uniform model predicts substantial syn-rift melting which is not observed.

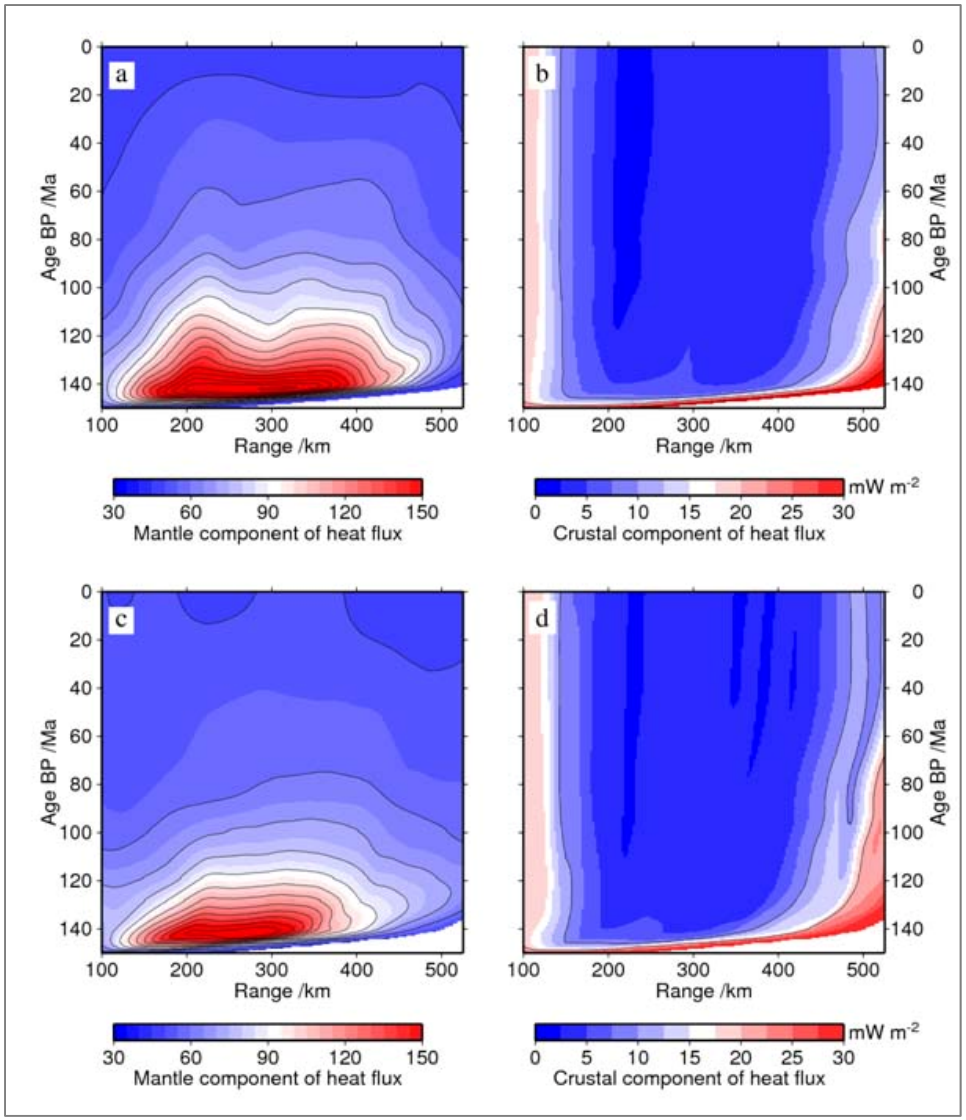

Figure 8. Heat flux corresponding to strain rate models in Figure 6. (a) Mantle heat flux for depth-uniform model. (b) Crustal heat flux for depth-uniform model assuming standard crustal composition. Total basement heat flux is the sum of these two components. (c) Mantle heat flux for depth-dependent model. Note how the lack of extension in the mantle near the ocean-continent transition reduces the mantle heat flux significantly compared to the uniform case in (a), which has implications for the maturation of pre-rift source rocks in similar highly-extended margins. (d) Crustal heat flux for depth-dependent model.

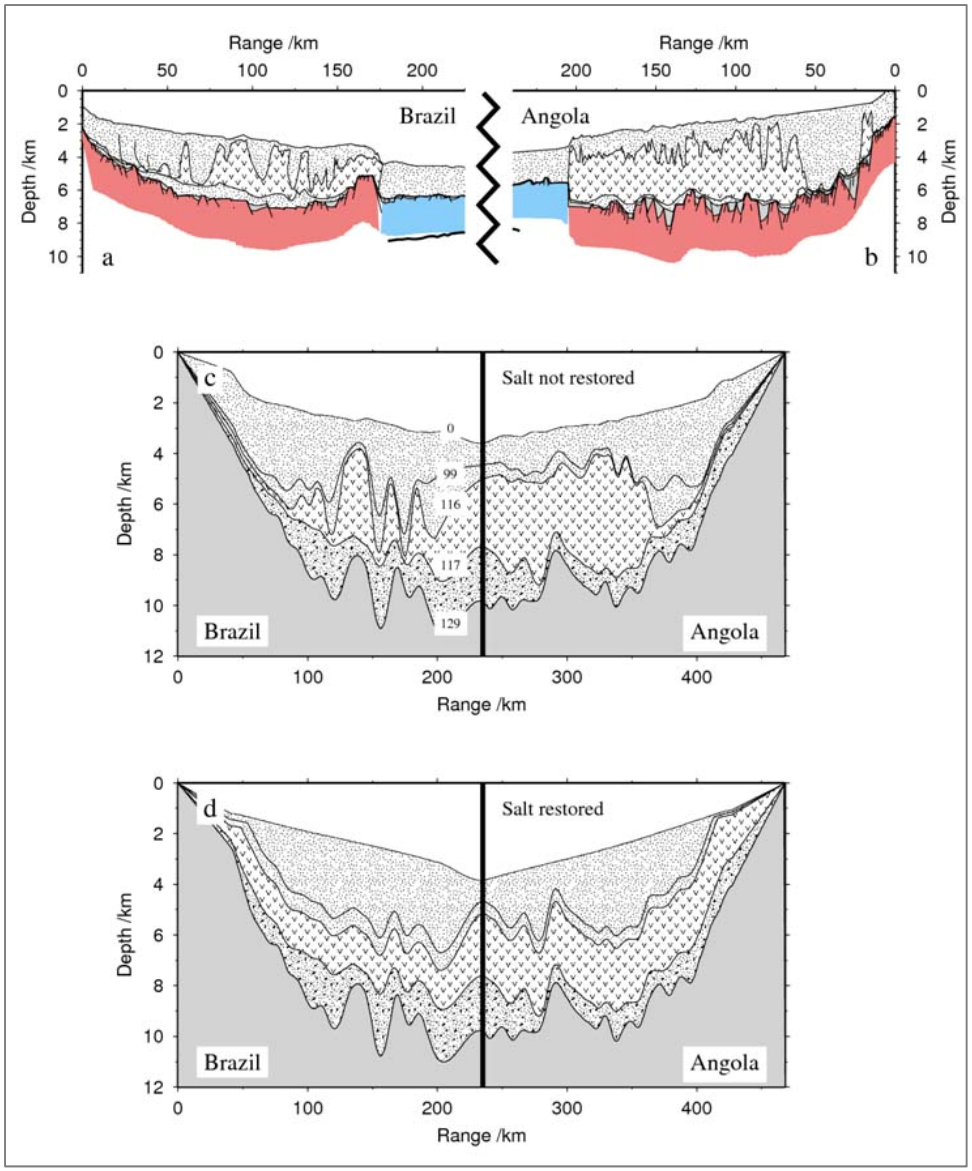

Figure 9. Santos-Kwanza (Brazil-Angola) conjugate margins. (a) Brazilian stratigraphy. Arrowheads = laterally translated massive salt. Fault interpretations sub-salt are speculative owing to poor seismic imaging. (b) Conjugate Angolan stratigraphy. (c) Joined conjugate profiles after correcting for differences in dynamic topography with stratigraphic ages in Ma. Presalt basins shown by heavy stipples. (d) Joined conjugate profiles with salt restored to uniform thickness and flexural loading correction applied. Stratigraphic thicknesses are smoothed at the join and tapered at each end.

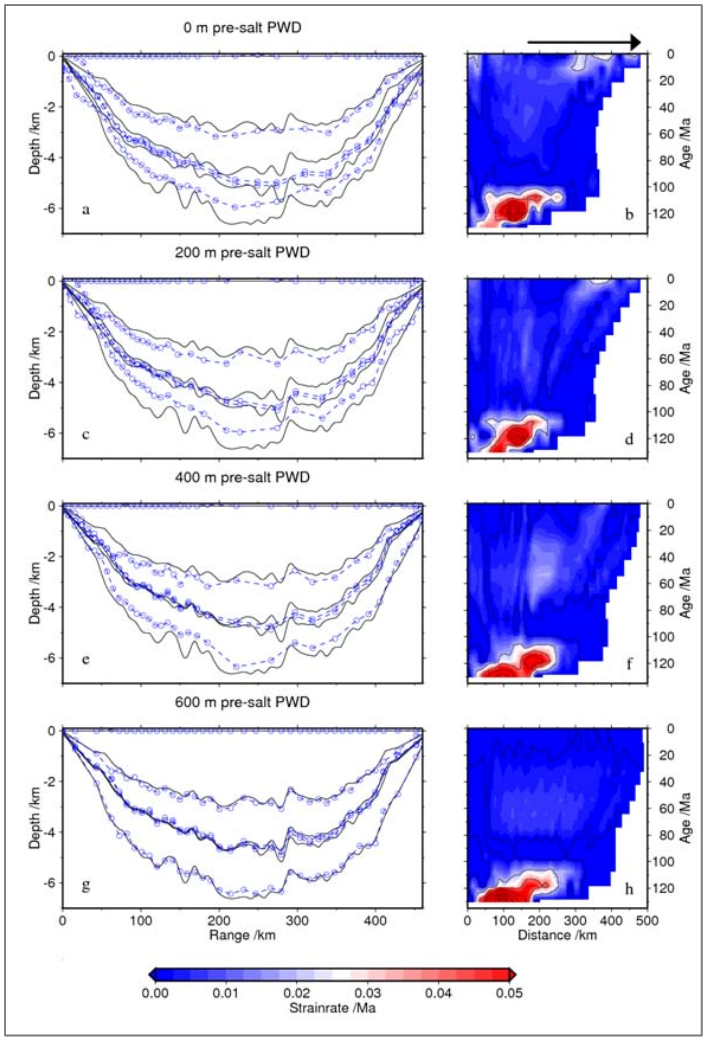

Figure 10. Fit to tectonic stratigraphy and strain rates as a function of time for the sedimentary stratigraphy shown in Figure 9d. Paleo-water depth at top salt is assumed to be zero and paleo-topography at base-salt is varied. (a, b) Base-salt paleo-topography is zero, implying deposition near sea level. Fit is poor and the strain rate cube shows late-stage strain incompatible with observed extensional faulting. (c, d) Base-salt paleo-topography is 200 m water-loaded equivalent. (e, f) Base-salt paleo-topography is 400 m water-loaded equivalent. (g, h) Base-salt paleo-topography is 600 m water-loaded equivalent. This model provides the best fit to the subsidence data and the most geologically sensible strain rate function given that normal faulting terminates below the base of the salt on both margins. The interpretation is that the salt represents passive infill of a pre-existing ~400 m topographic depression over a period of 1-2 Ma and resulted from periodic inundation and evaporation of invaded seawater, rather than a dramatic increase in subsidence of tectonic origin. Rifting was largely uniform with depth and had terminated prior to the accumulation of salt during Aptian times.

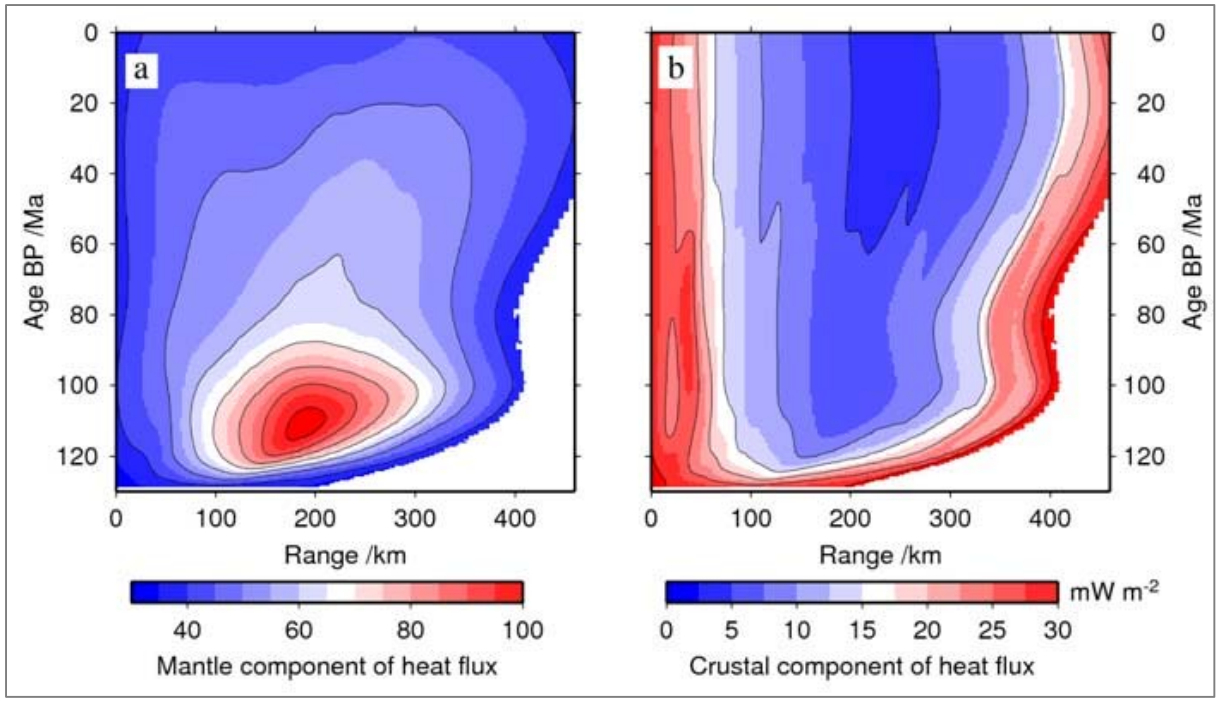

Figure 11. Heat flux versus time across the Brazil-Angola conjugate margins corresponding to the best-fit strain rate model in Figure 10h. Note that the heat flux evolution is relatively simple, and is close to what would be predicted using a simple 1D instantaneous stretching model (e.g. McKenzie, 1978).

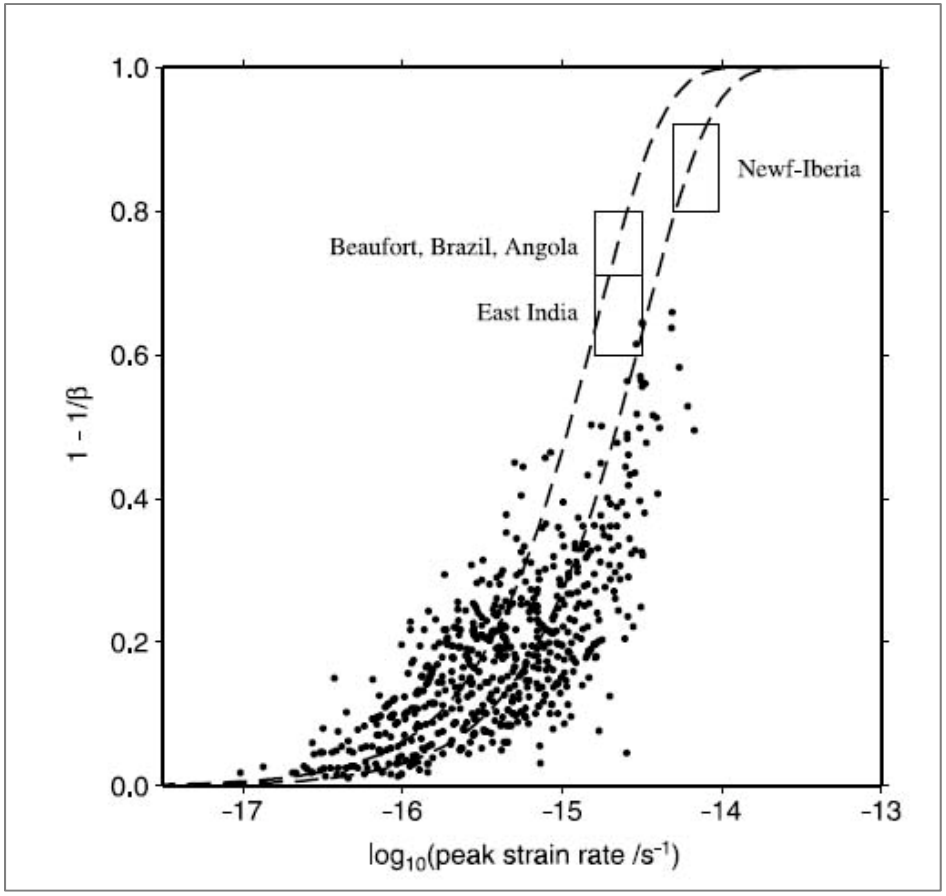

Figure 12. Peak strain rate as a function of extension factor. Solid circles = global database of 1D strain rate inversions from onshore and shallow water basins compiled by Newmann and White (1999), rectangles = results of this study, dashed lines = expected relationship for rift durations of 10 and 20 Ma. Note continuity of trend from mildly-extended sedimentary basins to highly-thinned deep-water margins.